Journal of Quality Measurement and Analysis *JQMA* 20(2) 2024, 111-125
e-ISSN: 2600-8602 *http://www.ukm.my/jqma*
https://doi.org/10.17576/jqma.2002.2024.09

COMPACTONS IN INTERSPECIES SPIN–ORBIT-COUPLED NONLINEAR SCHRÖDINGER LATTICES UNDER STRONG NONLINEARITY MANAGEMENT

(Kompakton dalam Kekisi Schrödinger Tak Linear yang Terganding Spin-Orbit Antaraspesis di Bawah Pengurusan Kuat Ketaklelurusan)

LUKHMAN ABDUL TAIB*, MUHAMMAD SALIHI ABDUL HADI & BAKHRAM UMAROV

ABSTRACT

This study shows the existence of special matter waves, known as compactons, in binary discrete nonlinear Schrödinger (DNLS) equations with equal distributions of interspecies Rashba and Dresselhaus spin-orbit coupling (SOC) in the presence of fast periodic time modulations of the interspecies scattering length. However, the existence is limited to only of one-site compacton type, which means the absence of larger size compactons such as the two- and three-site. Further, the dynamical stability of the compactons is predicted by using linear stability analysis method and verified through the direct numerical integrations of the equations. We find that the stability of the compactons has strong dependence on the strength of SOC term.

Keywords: discrete nonlinear Schrödinger equation, spin-orbit coupling, compactons, nonlinearity management

ABSTRAK

Kajian ini menunjukkan kewujudan gelombang jirim khas, yang dikenali sebagai kompakton, dalam persamaan dedua Schrödinger diskret tak linear bersama caruman sama gandingan spin-orbit Rashba dan Dresselhaus antaraspesis dengan kehadiran pemodulatan masa berkala pantas pada panjang serakan atom antara spesis. Namun, kewujudannya terhad kepada kompakton jenis bertapak satu, yang menunjukkan ketiadaan kompakton bersaiz besar seperti tapak dua dan tiga. Selanjutnya, kestabilan dinamik kompakton diramal menggunakan analisis kestabilan linear dan disahkan menerusi penyepaduan berangka langsung pada persamaan tersebut. Kami mendapati bahawa kestabilan kompakton amat bergantung dengan kekuatan sebutan gandingan spin-orbit.

Kata kunci: persamaan Schrödinger diskret tak linear, gandingan spin-orbit, kompakton, pengurusan ketaklelurusan

1. Introduction

One of the most intriguing outcomes of periodically managing parameters of a nonlinear system is the emergence of discrete breathers with unique localization properties (Malomed 2007). It is firmly established that the existence of discrete breathers depends on the interplay between discreteness, nonlinearity, and dispersion (Flach & Gorbach 2008). However, the presence of nonlinear dispersion causes the inter-site tunneling of excitations to vanish, resulting in the emergence of discrete breathers with no exponential tails, namely compactons (Rosenau & Hyman 1993; Rosenau 1994; Rosenau & Schochet 2005). Previous studies (Abdullaev *et al.* 2010, 2014, 2017; D'Ambroise *et al.* 2015) have demonstrated that the strong nonlinearity management (SNLM) technique, involving rapid periodic variations in nonlinearity, effectively induces the suppression of inter-site tunneling. This triggers compacton solutions in one- and two-component Bose-Einstein condensates (BECs) in optical lattices made of nonlinear optical waveguides. Compactons were predicted to exist not only in BECs under SNLM but also

in physical systems like exciton-polariton condensates (Kartashov *et al.* 2012), granular crystals with nonlinear interactions (English & Pego 2005; Stefanov & Kevrekidis 2012) and Lieb photonic lattices (Vicencio *et al.* 2015).

One possible method for achieving this periodic management is through Floquet engineering (FE). Theoretical and experimental studies on BECs based on FE have been carried out recently (see the review: Bukov *et al.* 2015). This technique is potent for manipulating quantum materials and involves controlling quantum systems using time-periodic external fields. Within the context of BECs, several approaches have been proposed to engineer effective magnetic fields based on driven cold-atom or ion-trap systems (Goldman & Dalibard 2014). These suggestions have led to a model that can be generalized as a lattice system penetrated by a uniform magnetic field. This encompasses both linear optical lattices (OL) achieved by periodically shaking the potential in time (either by adjusting amplitude or frequency) (Aidelsburger *et al.* 2011, 2013; Miyake *et al.* 2013; Aidelsburger *et al.* 2015) and nonlinear OL achieved by modulating the atom-atom interaction (Morsch & Oberthaler 2006). The linear scheme yields a modified hopping rate (Eckardt *et al.* 2005; Lignier *et al.* 2007; Kierig *et al.* 2008), which is useful, for instance, in driving transitions from a superfluid to a Mott insulator phase (Greiner *et al.* 2002; Zenesini *et al.* 2009), simulating frustrated classical magnetism (Struck *et al.* 2011), and creating synthetic gauge potentials (Struck *et al.* 2012). The nonlinear FE is implemented by introducing a modulated magnetic field close to a Feshbach resonance. This results in the hopping rate being dependent on the occupation differences at neighbouring sites (Gong *et al.* 2009; Rapp *et al.* 2012; Di Liberto *et al.* 2014).

Since the production of the first gaseous condensate in 1995 (Anderson *et al.* 1995), ultracold atoms, such as BECs and fermion gases, have been employed as physical simulators to study fundamental effects arising from condensed matter physics over the past decade (Bloch *et al.* 2008; Dalibard *et al.* 2011). One of these effects is spin-orbit coupling (SOC), which is described in quantum physics as the intrinsic interaction between particle dynamics and its spin. In the context of solid-state physics, SOC is the interaction between electron spin and its motion in a semiconductor, as elucidated by the works of Dresselhaus and Rashba (Elliott 1954; Dresselhaus *et al.* 1954; Dresselhaus 1955; Rashba 1959, 1960; Bychkov & Rashba 1984; Bihlmayer *et al.* 2015). Although SOC is weak and challenging to control in generic condensed matter materials due to its overshadowing by stronger electrostatic interactions, synthetic SOC can be induced in ultracold atoms and managed by external laser fields. This has been experimentally achieved for binary mixtures of BECs (Lin *et al.* 2011; Galitski & Spielman 2013).

Given that a variety of synthetic SOC can be engineered and controlled by external fields, particularly for binary mixtures of BECs, this area of study is currently attaining considerable attention. Models incorporating a spatial derivative of the SOC term, acting within each species and between species – known as intra- and inter-SOC, respectively – have been explored by (Beličev *et al.* 2015). The localization and spin dynamics (Zhang *et al.* 2021, 2022, 2023; Su *et al.* 2021; Wang *et al.* 2020, 2023; Guo *et al.* 2021; Luo *et al.* 2022; Mboumba *et al.* 2023; Zhu *et al.* 2023), modulational instability and formation of quantum droplets (Li *et al.* 2017; Cui 2018; Tononi *et al.* 2019; Ravisankar *et al.* 2020; Gangwar *et al.* 2022, 2023) in SOC-BEC have been reported. The effect of SOC and linear Zeeman splitting on the localized matter waves, particularly the symmetry breaking of solitons, has been investigated (Salerno & Abdullaev 2015; Wen *et al.* 2019), as well the correlation between SOC and the position changes in the Brillouin zone for generating superfluidity (Yu *et al.* 2018). The tunability of SOC in the presence of an external Zeeman field, varying periodically in time with strong modulation, also has been demonstrated in (Salerno *et al.* 2016). In higher dimensional solitons, SOC plays an important role of stabilizing in terms of suppressing the critical wave collapse (in 2D case) and 3D metastable solitons as a product of the interplay between the SOC and cubic self-attraction terms (Malomed 2022). Additionally, it is worth noting that the nonlinearity management of SOC-BEC results in certain manifestations of resonance between the time-periodic modulation of cubic attraction strength and intrinsic modes of the solitons (Sakaguchi & Malomed 2019).

Recently, it has been demonstrated that compactons exist in binary mixtures of BECs loaded

into a deep OL with intra-SOC under periodic time modulations of the intra-species scattering length (Abdullaev *et al.* 2023). This modulation leads to density-dependent SOC parameters that significantly affect the existence and stability of compactons. The presence of SOC terms restricts the parameter ranges within which stable compactons can exist; however, it provides a more distinct signature of their occurrence. Nonetheless, the potential existence and stability patterns of compactons in models with inter-species SOC remain open questions. This paper aims to investigate the existence of compactons in binary BEC systems described by discrete nonlinear Schrödinger (DNLS) equations, incorporating inter-SOC under the influence of SNLM. It is worth noting that the formation of compactons in the interspecies SOC model has been previously reported by Johansson *et al.* (2019). However, this paper introduces the concept of compact structures within localized modes achieved through the implementation of SNLM, a factor not explored by Johansson *et al.* (2019). Furthermore, the model utilized describes exciton-polaritons in a zigzag chain of weakly binary condensates with SOC, which differs from the model considered in this study.

This paper is organized as follows. In Section 2, we introduce the mathematical models representing binary BEC mixtures in a deep OL subjected to SNLM with SOC, and derived its effective average equations. In Section 3, we discuss the existence of SOC-compacton and its conditions. Numerical results for various cases of compactons are presented in Section 4 and their stability are evaluated by linear stability analysis and direct numerical integrations of the equations. Lastly, we summarize the main results in Section 5.

2. Model and Averaged Equations

A binary BEC mixture with equal contributions of interspecies Rashba and Dresselhaus SOC trapped in deep OL can be described by the following coupled DNLS equations (Beličev *et al.* 2015):

$$\begin{aligned} iu_{n,t} =& -\Gamma(u_{n+1}+u_{n-1}) + i\sigma(v_{n+1}-v_{n-1}) + \Omega u_n + (\gamma_1|u_n|^2+\gamma^{(0)}|v_n|^2)u_n, \\ iv_{n,t} =& -\Gamma(v_{n+1}+v_{n-1}) + i\sigma(u_{n+1}-u_{n-1}) - \Omega v_n + (\gamma^{(0)}|u_n|^2+\gamma_2|v_n|^2)v_n, \end{aligned} \tag{1}$$

where u_n, v_n are the pseudo-spinor complex wavefunctions at site n, the subscript t refers to the first derivative with respect to time, Γ denotes the inter-site hopping constant, σ and Ω are, respectively, the SOC and Zeeman splitting frequencies, and γ, γ_j, for $j = 1, 2$, indicate the nonlinear inter- and intraspecies interactions, respectively, in which we assume here to be attractive. Note that Eq. (1) possesses the Hamiltonian form $i\chi_{n,t} = \delta H/\delta\chi_n^*$ where the asterisk indicates the complex conjugate, with $\chi_n = u_n, v_n$ and Hamiltonian H in the form of:

$$\begin{aligned} H = \sum_n \Big[& -\Gamma(u_{n+1}u_n^* + u_{n+1}^* u_n) - \Gamma(v_{n+1}v_n^* + v_{n+1}^* v_n) \\ & + i\sigma(u_{n+1}v_n^* - u_{n+1}^* v_n) + i\sigma(v_{n+1}u_n^* - v_{n+1}^* u_n) \\ & + \Omega(|u_n|^2 - |v_n|^2) + \frac{1}{2}\left(\gamma_1|u_n|^4 + \gamma_2|v_n|^2\right) + \gamma|u_n|^2|v_n|^2\Big]. \end{aligned} \tag{2}$$

In the following, we consider mixtures of BEC species with interspecies NLM, i.e., fixed intraspecies nonlinearities ($\gamma_j = \text{const}$) and assume the interspecies nonlinear parameter $\gamma(t)$ modulated in the form of:

$$\gamma(t) \equiv \gamma^{(0)} + \gamma^{(1)}(t) = \gamma^{(0)} + \frac{\gamma^{(1)}}{\epsilon}\cos\left(\frac{\omega t}{\epsilon}\right),$$

with $\gamma^{(0)}$, $\gamma^{(1)}$ constants and ϵ a small paramater controling the strength of the management and

to separate the fast and slow time scales (SNLM requires $\epsilon \ll 1$). To eliminate the fast time, $\tau = t/\epsilon$, dependence, we perform the following transformation on Eq. (1):

$$u_n = U_n e^{-i\Lambda(\tau)|V_n|^2}, \quad v_n = V_n e^{-i\Lambda(\tau)|U_n|^2}, \tag{3}$$

where $\Lambda(\tau)$ indicates the antiderivatives of $\gamma^{(0)}(t)$, i.e., $\Lambda(\tau) \equiv \int_0^\tau (\gamma^{(1)}/\epsilon)\cos(\omega\tau')\, d\tau' = \alpha\sin(\omega\tau)$, with $\alpha = \gamma^{(1)}/\omega$. Substituting Eq. (3) into Eq. (1) yields:

$$\begin{aligned} iU_{n,t} = {} & i\Gamma\Lambda(\tau)U_n[X_{11}^* V_n - X_{11} V_n^*] - \sigma\Lambda(\tau)U_n[X_{21}^* V_n + X_{21} V_n^*] \\ & - \Gamma X_{22} + i\sigma X_{12} + \Omega U_n + [\gamma_1|U_n|^2 + \gamma^{(0)}|V_n|^2]U_n, \end{aligned} \tag{4a}$$

$$\begin{aligned} iV_{n,t} = {} & i\Gamma\Lambda(\tau)V_n[X_{22}^* U_n - X_{22} V_n^*] - \sigma\Lambda(\tau)V_n[X_{12}^* U_n + X_{12} V_n^*] \\ & - \Gamma X_{11} + i\sigma X_{21} - \Omega V_n + [\gamma^{(0)}|U_n|^2 + \gamma_2|V_n|^2]V_n, \end{aligned} \tag{4b}$$

where $X_{11} = V_{n+1}e^{-i\Lambda\theta_{11}^+} + V_{n-1}e^{-i\Lambda\theta_{11}^-}$, $X_{22} = U_{n+1}e^{-i\Lambda\theta_{22}^+} + U_{n-1}e^{-i\Lambda\theta_{22}^-}$, $X_{12} = V_{n+1}e^{-i\Lambda\theta_{12}^+} - V_{n-1}e^{-i\Lambda\theta_{12}^-}$, $X_{21} = U_{n+1}e^{-i\Lambda\theta_{21}^+} - U_{n-1}e^{-i\Lambda\theta_{21}^-}$, and:

$$\begin{aligned} \theta_{11}^\pm &= |U_{n\pm1}|^2 - |U_n|^2, \qquad \theta_{22}^\pm = |V_{n\pm1}|^2 - |V_n|^2, \\ \theta_{12}^\pm &= |U_{n\pm1}|^2 - |V_n|^2, \qquad \theta_{21}^\pm = |V_{n\pm1}|^2 - |U_n|^2. \end{aligned}$$

The average over the rapid modulation can be evaluated with the help of the following relation:

$$\langle \Lambda e^{\pm i\Lambda\theta^\pm}\rangle = \pm i\alpha J_1(\alpha\theta^\pm), \quad \langle e^{\pm i\Lambda\theta^\pm}\rangle = J_0(\alpha\theta^\pm), \tag{5}$$

where $\langle F\rangle$ indicates the average with respect to the rapid modulation, $\langle F\rangle \equiv (1/T)\int_0^T F\, d\tau$, and J_ν is Bessel function of the first kind of order ν with $\nu = 0, 1$. Substituting the averages into Eq. (4) yields the following system of averaged equations:

$$\begin{aligned} iU_{n,t} = {} & -\Gamma\big\{\alpha U_n\big[(V_{n+1}^* V_n + V_{n+1}V_n^*)J_1(\alpha\theta_{11}^+) + (V_{n-1}^* V_n + V_{n-1}V_n^*)J_1(\alpha\theta_{11}^-)\big] \\ & + U_{n+1}J_0(\alpha\theta_{22}^+) + U_{n-1}J_0(\alpha\theta_{22}^-)\big\} - i\sigma\big\{\alpha U_n\big[(U_{n+1}^* V_n - U_{n+1}V_n^*)J_1(\alpha\theta_{21}^+) \\ & - (U_{n-1}^* V_n - U_{n-1}V_n^*)J_1(\alpha\theta_{21}^-)\big] - V_{n+1}J_0(\alpha\theta_{12}^+) + V_{n-1}J_0(\alpha\theta_{12}^-)\big\} \\ & + \Omega U_n + \big[\gamma_1|U_n|^2 + \gamma^{(0)}|V_n|^2\big]U_n, \end{aligned} \tag{6a}$$

$$\begin{aligned} iV_{n,t} = {} & -\Gamma\big\{\alpha U_n\big[(U_{n+1}^* U_n + U_{n+1}U_n^*)J_1(\alpha\theta_{22}^+) + (U_{n-1}^* U_n + U_{n-1}U_n^*)J_1(\alpha\theta_{22}^-)\big] \\ & + V_{n+1}J_0(\alpha\theta_{11}^+) + V_{n-1}J_0(\alpha\theta_{11}^-)\big\} - i\sigma\big\{\alpha V_n\big[(V_{n+1}^* U_n - V_{n+1}U_n^*)J_1(\alpha\theta_{12}^+) \\ & - (V_{n-1}^* U_n - V_{n-1}U_n^*)J_1(\alpha\theta_{12}^-)\big] - U_{n+1}J_0(\alpha\theta_{21}^+) + U_{n-1}J_0(\alpha\theta_{21}^-)\big\} \\ & - \Omega V_n + \big[\gamma^{(0)}|U_n|^2 + \gamma_2|V_n|^2\big]V_n. \end{aligned} \tag{6b}$$

Note that the above system of averaged equations are valid only for $t \le 1/\epsilon$ with accuracy of $\mathcal{O}(\epsilon)$ (Sanders *et al.* 2007).

The averaged system Eq. (6) possesses a Hamiltonian form with the averaged Hamiltonian

$H_{\rm av}$ in the form of:

$$H_{\rm av} = \sum_n \Big\{ -\Gamma J_0(\alpha\theta_{22}^+)(U_{n+1}U_n^* + U_{n+1}^*U_n) - \Gamma J_0(\alpha\theta_{11}^+)(V_{n+1}V_n^* + V_{n+1}^*V_n) + i\sigma J_0(\alpha\theta_{21}^+)(U_{n+1}V_n^* - U_{n+1}^*V_n) + i\sigma J_0(\alpha\theta_{12}^+)(V_{n+1}U_n^* - V_{n+1}^*U_n) + \Omega\big[|U_n|^2 - |V_n|^2\big] + \frac{1}{2}\big[\gamma_1|U_n|^4 + \gamma_2|V_n|^4\big] + \gamma^{(0)}|U_n|^2|V_n|^2 \Big\}. \tag{7}$$

By comparing $H_{\rm av}$ in Eq. (7) with the corresponding original Hamiltonian in Eq. (2), we can see that they coincide if we rescale the tunnelling constant Γ and the SOC parameter σ according to:

$$\Gamma \to \tilde{\Gamma}_i \equiv \Gamma J_0(\alpha\theta_{ij}^+), \quad (i = j),$$
$$\sigma \to \tilde{\sigma}_i \equiv \sigma J_0(\alpha\theta_{ij}^+), \quad (i \neq j),$$

for $i = 1, 2$ and $j = 1, 2$. From this, we see that the modulation of interspecies scattering interaction introduces a dependence on the density imbalance between adjacent sites of the same component for Γ and between the two components for σ in the unmodulated system. It becomes obvious that the condition of the existence of compacton, i.e. zero tunnelling rate at compacton edges, does not only involves the intersite hopping constant Γ but also the SOC parameter σ.

3. The Existence and Stability of SOC-Compactons

In this section, we derive steady-state SOC-compacton solutions in order to establish the stationary conditions for their existence. Stationary compacton solutions of the averaged system can be searched in the form of:

$$U_n = A_n e^{-i\mu t}, \qquad V_n = B_n e^{-i\mu t}, \tag{8}$$

with A_n, B_n complex amplitudes and μ chemical potential for the two components. Substituting Eq. (8) into the averaged system (6) leads to the following steady-state equations:

$$\mu A_n = F_1, \qquad \mu B_n = F_2, \tag{9}$$

to be solved for the amplitudes A_n, B_n and chemical potential, where F_1 and F_2 stands for the right hand side of Eqs. (6a) and (6b), respectively, but with the replacements $U_n \to A_n$ and $V_n \to B_n$.

In order to obtain the conditions for the existence of stationary SOC-compactons, we adopt the following ansatz:

$$A_n, B_n \neq 0 \quad \text{if } n_0 \leq n \leq n_0 + s,$$
$$A_n, B_n = 0 \quad \text{otherwise}, \tag{10}$$

with n_0 and $n_0 + s$ left and right edges of the compactons, respectively, and s its width. The compact nature of the solution allows us to reduce the above infinite system into $2(s + 3)$ equations by substituting the ansatz (10) into Eq. (9). The existence of compactons depends on the likelihood to solve these equations for nonzero amplitudes by achieving both the suppression of tunnelling rate at the edges and deriving expressions for the chemical potential.

The dynamical stability of SOC-compactons in the system (6) can be predicted by employing

the conventional linear stability analysis procedure by taking the perturbed ansatz of the form:

$$U_n = \left[A_n + \varepsilon(a_n e^{-i\lambda t} + b_n e^{i\lambda^* t})\right] e^{-i\mu t},$$
$$V_n = \left[B_n + \varepsilon(c_n e^{-i\lambda t} + d_n e^{i\lambda^* t})\right] e^{-i\mu t}, \tag{11}$$

where $\lambda = \lambda_r + i\lambda_i$ indicates the linearization eigenvalue and $\varepsilon \ll 1$. Substituting the ansatz (11) into Eq. (6), and taking only the terms with $\mathcal{O}(\varepsilon)$, leads to an eigenvalue problems for λ, which can be solved numerically. Stable compacton solutions should be indicated by the absence (or negligibly small value) of imaginary parts of λ, for gain $G = \max(|\lambda_i|) \simeq 0$. However, in this case, the eigenvalue problem possesses high sensitivity which lead to small gain of unstable solutions, hence enhancement to the computation of gain will be required, and it will be elaborated in the next section.

The stability prediction is verified through direct numerical integrations of Eqs. (6) and (1) by utilising Runge-Kutta-Fehlberg (RK45) method of fourth-fifth order. The initial conditions of the solutions are taken from the stationary profiles of Eq. (9) with additional uniformly-distributed random perturbation of 10^{-4}.

4. Numerical Results and Discussions

4.1. *One-site compactons*

One-site compactons in the inter-SOC model can be sought by fixing $s = 0$ in Eq. (10) and taking the ansatz at site n_0 as $A_{n_0} = z_1 \equiv a + ib$ and $B_{n_0} = z_2 \equiv c + id$, with a, b, c, d reals. By substituting the ansatz into Eq. (9), we obtain four equations corresponding to the compactons edges $n_0 \pm 1$, which are automatically satisfied if $J_0\big(\alpha\big(a^2 + b^2\big)\big) = 0$ and $J_0\big(\alpha\big(c^2 + d^2\big)\big) = 0$, i.e. if a, b, c and d are taken as:

$$a^2 + b^2 = \frac{\xi_m}{\alpha}, \quad c^2 + d^2 = \frac{\xi_l}{\alpha}, \qquad (m, l = 1, 2, \dots) \tag{12}$$

where ξ_m, ξ_l are zeros of the Bessel function J_0. The remaining two equations yield the expression for chemical potential:

$$\mu = \gamma^{(0)} \frac{\xi_m}{\alpha} + \gamma_2 \frac{\xi_l}{\alpha} - \Omega, \tag{13}$$

where the Zeeman splitting term, Ω, is defined as:

$$\Omega = \frac{1}{2\alpha}\left[\left(\gamma_2 - \gamma^{(0)}\right)\xi_l - \left(\gamma_1 - \gamma^{(0)}\right)\xi_m\right]. \tag{14}$$

Since the two zeros of J_0 in Eq. (12) should not be necessarily equal, this implies that the densities at excited site n_0 of the two species could either be balanced or unbalanced.

Let us begin examining one-site compactons cases with parameters $\Gamma \in [0, 1]$, $\sigma = 1$, $\gamma_1 = \gamma_2 = \gamma^{(0)} \equiv -1, \gamma^{(1)} = 1$, $\omega = 1$ and $\Omega = 0$. As for the excited states at lattice number $n = 0$, we choose $A_0 = B_0 \equiv a + ib$ where $a = 0.5\sqrt{\xi_1/\alpha}$ and $b = \sqrt{\xi_1/\alpha - a^2}$ with $\xi_1 = 2.4048$ (first root of J_0), in such a way that the magnitude will conform with the solution ξ_1/α. The numerical result is shown in Figure 1, where from panel (d) the gain G is notably small on order of $\mathcal{O}(10^{-7})$. To facilitate the analysis, it is convenient to consider $G(\Gamma)$ in the form of base 10 logarithm, $G_{10}(\Gamma) = \log_{10}(G(\Gamma))$, in which giving us the value $G_{10}(\Gamma) = -7.1277$ at $\Gamma = 1$. We then increase the value of σ to 5 and the result is displayed in Figure 2, where the gain G remains small on the order of $\mathcal{O}(10^{-7})$, not significantly different from the previous case with $\sigma = 1$. However, in this case, $G_{10}(1)$ assumes the value of -6.3567. Based on the

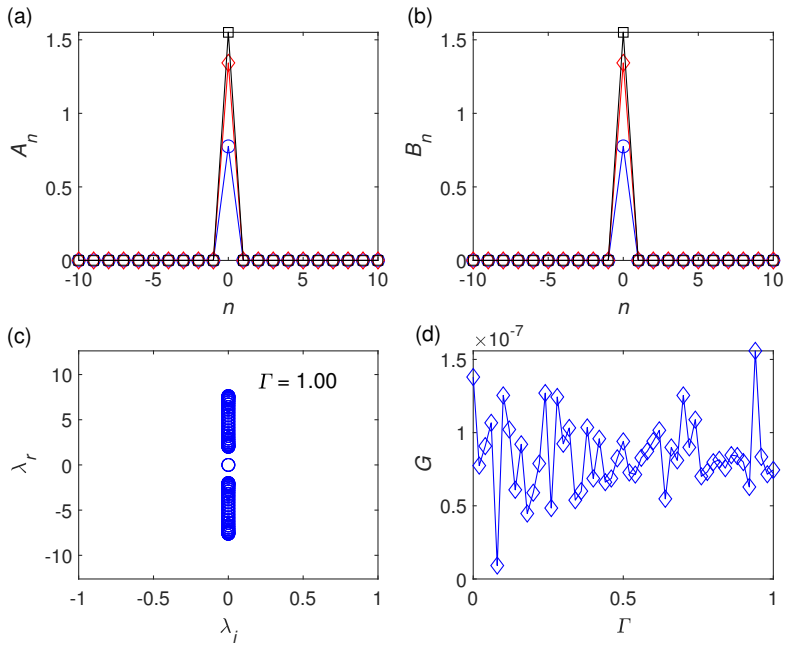

Figure 1: *Top row panels:* Steady-state solution profiles for one-site compactons with parameters $\Gamma \in [0, 1]$, $\sigma = 1$, $\gamma_1 = \gamma_2 = \gamma^{(0)} \equiv -1$, $\gamma^{(1)} = 1$, $\omega = 1$ and $\Omega = 0$, with $|A_0|^2 = |B_0|^2 \equiv 2.4048$. Blue (circle), red (diamond) and black (square) lines denote real and imaginary parts and the absolute value of the amplitudes, respectively. *Bottom row panels:* the plane (λ_i, λ_r) of the linearization eigenvalues $\lambda = \lambda_r + i\lambda_i$ (left panel) and the gain G as a function of Γ (right panel).

small order of gain, it looks like in both cases, the one-site compactons should be stable. In order to verify this analysis, we directly integrate the original and averaged equations for both scenarios, presenting the results in Figure 3 and 4, respectively. The space-time evolution for $\sigma = 1$ case shows stability in both original and averaged equations, as demonstrated in Figure 3. However, in the case of $\sigma = 5$, the compactons completely disperse in time, as shown in Figure 4. This indicates that an increase in σ contributes to instability despite the gain being close to zero. Nevertheless, a lower value of σ appears to result in approximately lower gain of $\mathcal{O}(10^{-1})$, which is sufficient to justify stability.

We repeated the same procedure but changed $B_0 = c + id$, where $c = 0.5\sqrt{\xi_2/\alpha}$ and $d = \sqrt{\xi_2/\alpha - c^2}$ with $\xi_2 = 5.5201$ (second root of J_0), ensuring that the magnitude of compacton at the second lattice corresponds to ξ_2/α. The results, while not displayed here, were found to be similar to the case of balanced density presented in Figures 1-4, except for the magnitude $|B_0| = 2.3495$, which is higher than $|A_0| = 1.5507$. In the instance of $\sigma = 1$, we observe that $G_{10}(1) = -7.4698$, and for $\sigma = 5$ it takes the value of $G_{10}(1) = -6.6129$, once again justifying the stability of compactons for lower values of SOC strength. It can also be deduced that the unbalanced densities of atoms between the binary lattices do not affect the stability, at least for the case of one-site compacton. It is suggested that a critical point may exist, distinguishing the range of stability, as it becomes evident here that the compactons are stable when $G_{10}(1) < -7$.

4.2. *Two-site compactons*

The scenario of two-site compactons in the inter-SOC model yields a peculiar result. Let us begin by fixing $s = 1$ in Eq. (10) and taking the ansatz $A_{n_0} = A^*_{n_0+1} \equiv z_1$ and $B^*_{n_0} = B_{n_0+1} \equiv z_2$ with z_1, z_2 complex amplitudes. Then, we obtain eight equations corresponding

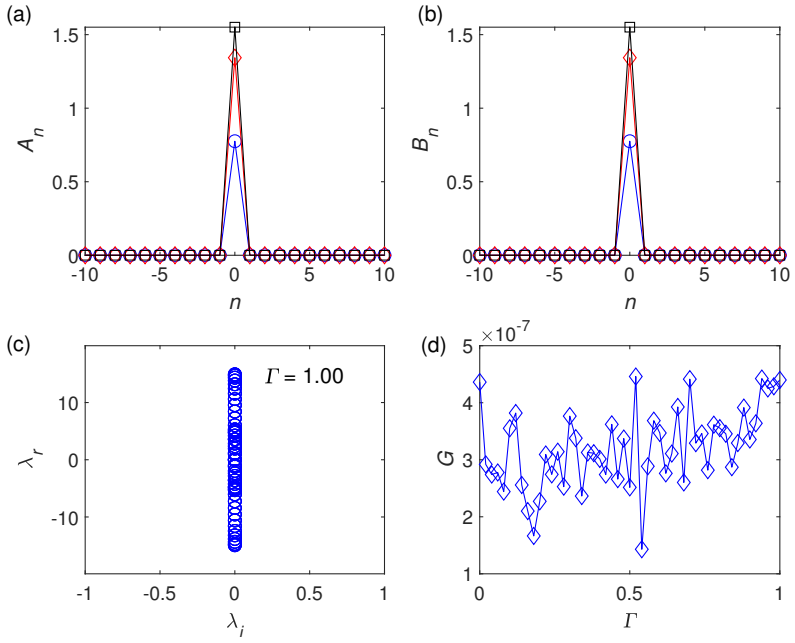

Figure 2: Similar as in Figure 1, except for one-site compactons with SOC parameter $\sigma = 5$. Other parameters are fixed as in Figure 1.

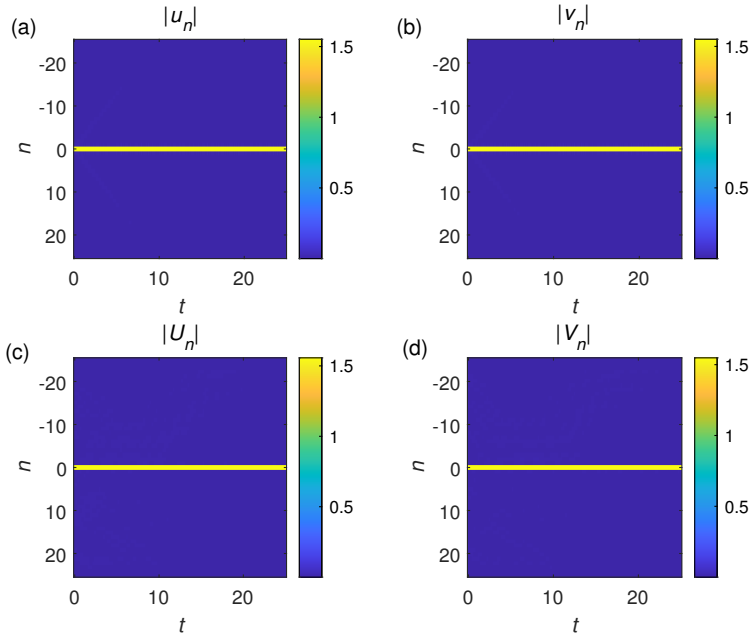

Figure 3: Space-time evolution of one-site compactons in correspondence to parameters as in Figure 1 by performing the direct numerical integration on Eqs. (2) (*top row panels*) and (6) (*bottom row panels*) with $\epsilon = 1/200$.

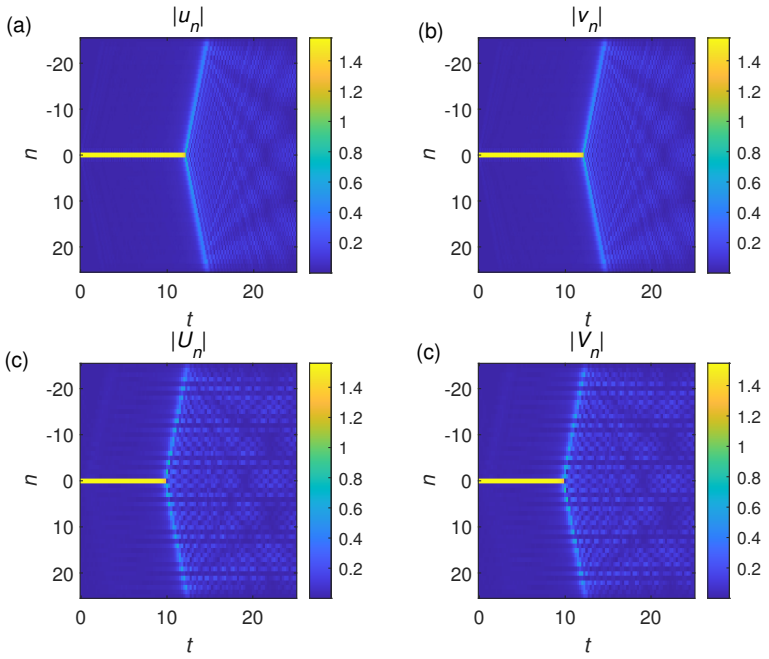

Figure 4: Space-time evolution of Eqs. (2) and (6) for one-site compactons with $\sigma = 5$ and $\epsilon = 1/200$. Other parameters are fixed as in Figure 2.

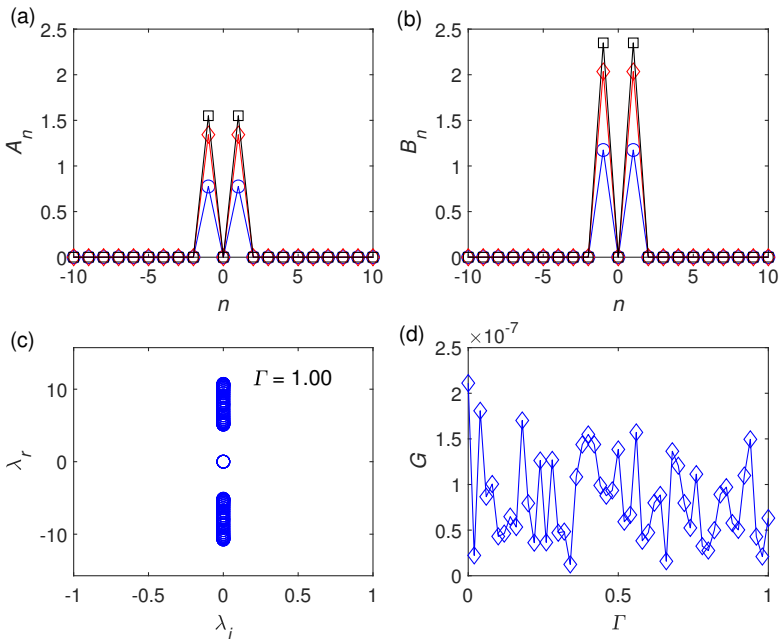

Figure 5: Similar as in Figure 1 but for double one-site compactons with $|A_{\pm 1}|^2 = 2.4048$ and $|B_{\pm 1}|^2 = 5.5201$. All parameters as fixed as in Figure 1.

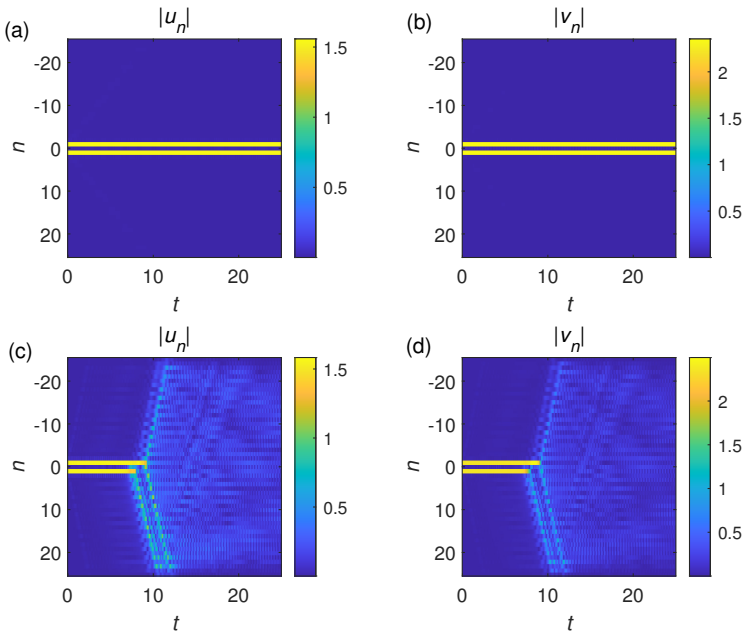

Figure 6: Space-time evolution of Eq. (2) for double one-site compactons, with $\sigma = 1$ (*top row panels*), $\sigma = 5$ (*bottom row panels*) and $\epsilon = 1/200$. Other parameters are fixed as in Figure 1.

to sites $n_0 - 1$, n_0, $n_0 + 1$ and $n_0 + 2$ after substituting the ansatz into Eq. (9). The conditions for the compacton existence can be obtain if the equations in correspondence of the compacton edges $n_0 - 1$ and $n_0 + 2$ satisfy $J_0\left(|z_1|^2\right) = 0$ and $J_0\left(|z_2|^2\right) = 0$, thus:

$$|z_1|^2 = \frac{\xi_m}{\alpha}, \quad |z_2|^2 = \frac{\xi_l}{\alpha}, \tag{15}$$

with ξ_m, ξ_l zeros of J_0. The remaining four equations corresponding to sites n_0 and $n_0 + 1$ can be simplified and reduced into two equations:

$$\begin{aligned} &\Gamma z_1^* - i\alpha\sigma z_1 \left(z_1 z_2^* - z_1^* z_2\right) J_1\left[\alpha\left(|z_2|^2 - |z_1|^2\right)\right] + i\sigma z_2 J_0\left[\alpha\left(|z_1|^2 - |z_2|^2\right)\right] = 0, \\ &\Gamma z_2^* + i\alpha\sigma z_2 \left(z_1^* z_2 - z_1 z_2^*\right) J_1\left[\alpha\left(|z_1|^2 - |z_2|^2\right)\right] - i\sigma z_1 J_0\left[\alpha\left(|z_2|^2 - |z_1|^2\right)\right] = 0. \end{aligned} \tag{16}$$

However, Eq. (16) only has trivial solutions, i.e. all zeros, which contradicts to the existence conditions given in (15); this implies furthermore the absence of two-site compactons in the inter-SOC system as oppose to the intra-SOC model reported by Abdullaev *et al.* (2023). Since this analytically justifies the nonexistence of the two-site compactons, hence finding the numerical solutions would be unnecessary.

4.3. *Three-site compactons*

As for three-site compactons in inter-SOC model, we fix $s = 2$ in (10) and substituting the following ansatz $A_{n_0} = z_1$, $A_{n_0 \pm 1} = z_2$, $B_{n_0} = w_1$ and $B_{n_0 \pm 1} = w_2$ into Eq. (9), with complex fields z_1, z_2, w_1 and w_2. Four equations in correspondence to the compacton edges $n_0 \pm 2$ are automatically satisfied if $J_0\left(\alpha|z_2|^2\right) = 0$ and $J_0\left(\alpha|w_2|^2\right) = 0$, i.e. if z_2 and w_2 are

taken as:

$$|z_2|^2 = \frac{\xi_m}{\alpha}, \quad |w_2|^2 = \frac{\xi_l}{\alpha}, \tag{17}$$

again, ξ_m, ξ_l are zeros of J_0. Another four equations corresponding to sites $n_0 \pm 1$ have the same form to the ones for one-site compactons at site n_0 with additional terms which are equal to zero in the one-site case:

$$\begin{aligned}
&-\Gamma z_1 J_0\left[\alpha(|w_1|^2-|w_2|^2)\right] + i\sigma w_1 J_0\left[\alpha(|z_1|^2-|w_2|^2)\right] \\
&\quad -\alpha z_2\left\{\Gamma(w_1^* w_2 + w_1 w_2^*) J_1\left[\alpha(|z_1|^2-|z_2|^2)\right]\right. \\
&\quad \left. + i\sigma(z_1^* w_2 - z_1 w_2^*) J_1\left[\alpha(|w_1|^2-|z_2|^2)\right]\right\} = 0, \qquad (18)\\
&-\Gamma w_1 J_0\left[\alpha(|z_1|^2-|z_2|^2)\right] + i\sigma z_1 J_0\left[\alpha(|w_1|^2-|z_2|^2)\right] \\
&\quad -\alpha w_2\left\{\Gamma(z_1^* z_2 + z_1 z_2^*) J_1\left[\alpha(|w_1|^2-|w_2|^2)\right]\right. \\
&\quad \left. + i\sigma(w_1^* z_2 - w_1 z_2^*) J_1\left[\alpha(|z_1|^2-|w_2|^2)\right]\right\} = 0, \qquad (19)\\
&-\Gamma z_1 J_0\left[\alpha(|w_1|^2-|w_2|^2)\right] - i\sigma w_1 J_0\left[\alpha(|z_1|^2-|w_2|^2)\right] \\
&\quad -\alpha z_2\left\{\Gamma(w_1^* w_2 + w_1 w_2^*) J_1\left[\alpha(|z_1|^2-|z_2|^2)\right]\right. \\
&\quad \left. - i\sigma(z_1^* w_2 - z_1 w_2^*) J_1\left[\alpha(|w_1|^2-|z_2|^2)\right]\right\} = 0, \qquad (20)\\
&-\Gamma w_1 J_0\left[\alpha(|z_1|^2-|z_2|^2)\right] - i\sigma z_1 J_0\left[\alpha(|w_1|^2-|z_2|^2)\right] \\
&\quad -\alpha w_2\left\{\Gamma(z_1^* z_2 + z_1 z_2^*) J_1\left[\alpha(|w_1|^2-|w_2|^2)\right]\right. \\
&\quad \left. - i\sigma(w_1^* z_2 - w_1 z_2^*) J_1\left[\alpha(|z_1|^2-|w_2|^2)\right]\right\} = 0. \qquad (21)
\end{aligned}$$

However, solving Eqs. (18)-(21) yields trivial solutions for z_1 and w_1. This leads the collapse of the middle peak of the three-site compactons to become two one-site compactons, instead.

The double one-site compactons cases are treated exactly as the one-site cases, as both the amplitudes of excitations and the chemical potential follow the same formulation in Eqs. (12) and (13), respectively. In the first scenario with $\sigma = 1$ and balanced densities $A_{\pm 1} = B_{\pm 1}$, we obtained $G_{10}(1) = -6.9854$, while for $\sigma = 5$, it was $G_{10}(1) = -6.6598$. The direct numerical integration of both original and averaged equations demonstrated stability for case $\sigma = 1$ but not in the case of $\sigma = 5$. To preserve brevity of this paper, these results will not be shown here since they are already well covered in subsection 4.1.

As for the case of unbalanced densities, $A_{\pm 1} \neq B_{\pm 1}$, with $\sigma = 1$, the result for steady state solution is illustrated in Figure 5 where $G_{10}(1) = -7.1993$, while for $\sigma = 5$ we obtained $G_{10}(1) = -6.7939$, though the plot is not displayed. In Figure 6 we exhibit the direct numerical integration results for the original equations, with the upper and lower panels representing $\sigma = 1$ and $\sigma = 5$ cases, respectively. Evidently, the double one-site compactons are stable in the former case but unstable in the latter, and one could arrive at the assumption that critical point for the gain is about $G_{10}(1) = -6.9$, which is also consistent with the one-site compacton scenarios.

5. Conclusion

In this paper we have demonstrated the existence of compactons in binary BEC mixtures with interspecies spin-orbit interaction, trapped in a deep OL under SNLM governed by coupled DNLS equations. The corresponding effective averaged system has been derived and based on the tunneling suppression phenomenon that defined compactons, the steady state of the infinite averaged system can be reduced into some set of finite algebraic equations where the analytical solution for the compactons can be determined. Apparently for this model, the type of

compactons that could be found are the one-site profiles and the multiples of this type. Interestingly, these type of compactons support the existence of unbalanced densities between the species. However, the stability of compactons is not affected by the density imbalance of the two species, but rather the strength of SOC term itself. Modifications on the linear stability analysis reveals there exists a critical point for the gain in which the compactons becomes unstable when it exceeds the critical point. This can be further verified by directly solve the original DNLS equations with small perturbation where the unstable compactons disperse along transient.

Acknowledgment

This research is supported by International Islamic University Malaysia (IIUM) and the Ministry of Higher Education (MOHE), Malaysia under research grant no. FRGS 16-013-0512.

References

Abdullaev F.K., Hadi M.S.A., Salerno M. & Umarov B. 2014. Compacton matter waves in binary Bose gases under strong nonlinear management. *Physical Review A* **90**(6): 063637.

Abdullaev F.K., Hadi M.S.A., Salerno M. & Umarov B.A. 2017. Binary matter-wave compactons induced by interspecies scattering length modulations. *Journal of Physics B: Atomic, Molecular and Optical Physics* **50**(16): 165301.

Abdullaev F.K., Hadi M.S.A., Umarov B., Taib L.A. & Salerno M. 2023. Compacton existence and spin-orbit density dependence in Bose-Einstein condensates. *Physical Review E* **107**(4): 044218.

Abdullaev F.K., Kevrekidis P.G. & Salerno M. 2010. Compactons in nonlinear Schrödinger lattices with strong nonlinearity management. *Physical Review Letters* **105**(11): 113901.

Aidelsburger M., Atala M., Lohse M., Barreiro J.T., Paredes B. & Bloch I. 2013. Realization of the Hofstadter Hamiltonian with ultracold atoms in optical lattices. *Physical Review Letters* **111**(18): 185301.

Aidelsburger M., Atala M., Nascimbene S., Trotzky S., Chen Y.A. & Bloch I. 2011. Experimental realization of strong effective magnetic fields in an optical lattice. *Physical Review Letters* **107**(25): 255301.

Aidelsburger M., Lohse M., Schweizer C., Atala M., Barreiro J.T., Nascimbène S., Cooper N., Bloch I. & Goldman N. 2015. Measuring the Chern number of Hofstadter bands with ultracold bosonic atoms. *Nature Physics* **11**(2): 162–166.

Anderson M.H., Ensher J.R., Matthews M.R., Wieman C.E. & Cornell E.A. 1995. Observation of Bose-Einstein condensation in a dilute atomic vapor. *Science* **269**(5221): 198–201.

Beličev P.P., Gligorić G., Petrovic J., Maluckov A., Hadžievski L. & Malomed B.A. 2015. Composite localized modes in discretized spin–orbit-coupled Bose–Einstein condensates. *Journal of Physics B: Atomic, Molecular and Optical Physics* **48**(6): 065301.

Bihlmayer G., Rader O. & Winkler R. 2015. Focus on the Rashba effect. *New Journal of Physics* **17**(5): 050202.

Bloch I., Dalibard J. & Zwerger W. 2008. Many-body physics with ultracold gases. *Reviews of Modern Physics* **80**(3): 885.

Bukov M., D'Alessio L. & Polkovnikov A. 2015. Universal high-frequency behavior of periodically driven systems: from dynamical stabilization to Floquet engineering. *Advances in Physics* **64**(2): 139–226.

Bychkov Y.A. & Rashba E.I. 1984. Oscillatory effects and the magnetic susceptibility of carriers in inversion layers. *Journal of Physics C: Solid State Physics* **17**(33): 6039.

Cui X. 2018. Spin-orbit-coupling-induced quantum droplet in ultracold Bose-Fermi mixtures. *Physical Review A* **98**(2): 023630.

Dalibard J., Gerbier F., Juzeliūnas G. & Öhberg P. 2011. Colloquium: Artificial gauge potentials for neutral atoms. *Reviews of Modern Physics* **83**(4): 1523.

D'Ambroise J., Salerno M., Kevrekidis P.G. & Abdullaev F.K. 2015. Multidimensional discrete compactons in nonlinear Schrödinger lattices with strong nonlinearity management. *Physical Review A* **92**(5): 053621.

Di Liberto M., Creffield C.E., Japaridze G. & Smith C.M. 2014. Quantum simulation of correlated-hopping models with fermions in optical lattices. *Physical Review A* **89**(1): 013624.

Dresselhaus G. 1955. Spin-orbit coupling effects in zinc blende structures. *Physical Review* **100**(2): 580.

Dresselhaus G., Kip A. & Kittel C. 1954. Spin-orbit interaction and the effective masses of holes in germanium. *Physical Review* **95**(2): 568.

Eckardt A., Weiss C. & Holthaus M. 2005. Superfluid-insulator transition in a periodically driven optical lattice. *Physical Review Letters* **95**(26): 260404.

Elliott R. 1954. Spin-orbit coupling in band theory—character tables for some "double" space groups. *Physical Review* **96**(2): 280.

English J. & Pego R. 2005. On the solitary wave pulse in a chain of beads. *Proceedings of the American Mathematical Society* **133**(6): 1763–1768.

Flach S. & Gorbach A.V. 2008. Discrete breathers—advances in theory and applications. *Physics Reports* **467**(1 - 3): 1 – 116.

Galitski V. & Spielman I.B. 2013. Spin–orbit coupling in quantum gases. *Nature* **494**(7435): 49–54.

Gangwar S., Ravisankar R., Mistakidis S., Muruganandam P. & Mishra P.K. 2023. Spectrum and quench-induced dynamics of spin-orbit coupled quantum droplets. *arXiv preprint arXiv:2307.16742* .

Gangwar S., Ravisankar R., Muruganandam P. & Mishra P.K. 2022. Dynamics of quantum solitons in Lee-Huang-Yang spin-orbit-coupled Bose-Einstein condensates. *Physical Review A* **106**(6): 063315.

Goldman N. & Dalibard J. 2014. Periodically driven quantum systems: effective Hamiltonians and engineered gauge fields. *Physical Review X* **4**(3): 031027.

Gong J., Morales-Molina L. & Hänggi P. 2009. Many-body coherent destruction of tunneling. *Physical Review Letters* **103**(13): 133002.

Greiner M., Mandel O., Esslinger T., Hänsch T.W. & Bloch I. 2002. Quantum phase transition from a superfluid to a Mott insulator in a gas of ultracold atoms. *Nature* **415**(6867): 39–44.

Guo H., Qiu X., Ma Y., Jiang H.F. & Zhang X.F. 2021. Dynamics of bright soliton in a spin–orbit coupled spin-1 Bose–Einstein condensate. *Chinese Physics B* **30**(6): 060310.

Johansson M., Beličev P.P., Gligorić G., Gulevich D.R. & Skryabin D.V. 2019. Nonlinear gap modes and compactons in a lattice model for spin-orbit coupled exciton-polaritons in zigzag chains. *Journal of Physics Communications* **3**(1): 015001.

Kartashov Y.V., Konotop V.V. & Torner L. 2012. Compactons and bistability in exciton-polariton condensates. *Physical Review B* **86**(20): 205313.

Kierig E., Schnorrberger U., Schietinger A., Tomkovic J. & Oberthaler M. 2008. Single-particle tunneling in strongly driven double-well potentials. *Physical Review Letters* **100**(19): 190405.

Li Y., Luo Z., Liu Y., Chen Z., Huang C., Fu S., Tan H. & Malomed B.A. 2017. Two-dimensional solitons and quantum droplets supported by competing self-and cross-interactions in spin-orbit-coupled condensates. *New Journal of Physics* **19**(11): 113043.

Lignier H., Sias C., Ciampini D., Singh Y., Zenesini A., Morsch O. & Arimondo E. 2007. Dynamical control of matter-wave tunneling in periodic potentials. *Physical Review Letters* **99**(22): 220403.

Lin Y.J., Jiménez-García K. & Spielman I.B. 2011. Spin–orbit-coupled Bose–Einstein condensates. *Nature* **471**(7336): 83–86.

Luo H.B., Malomed B.A., Liu W.M. & Li L. 2022. Bessel vortices in spin-orbit-coupled binary Bose–Einstein condensates with Zeeman splitting. *Communications in Nonlinear Science and Numerical Simulation* **115**: 106769.

Malomed B.A. 2007. *Soliton Management in Periodic Systems*. Berlin: Springer-Verlag.

Malomed B.A. 2022. *Multidimensional Solitons*. New York: AIP Publishing Books.

Mboumba M.D., Makoundit G.J.N., Sadem C.K., Moubissi A.B. & Kofané T.C. 2023. Soliton molecules in coupled dipolar Bose–Einstein condensates with spin-orbit coupling. *Modern Physics Letters B* p. 2350075.

Miyake H., Siviloglou G.A., Kennedy C.J., Burton W.C. & Ketterle W. 2013. Realizing the Harper Hamiltonian with laser-assisted tunneling in optical lattices. *Physical Review Letters* **111**(18): 185302.

Morsch O. & Oberthaler M. 2006. Dynamics of Bose-Einstein condensates in optical lattices. *Reviews of Modern Physics* **78**(1): 179.

Rapp Á., Deng X. & Santos L. 2012. Ultracold lattice gases with periodically modulated interactions. *Physical Review Letters* **109**(20): 203005.

Rashba E. 1959. Symmetry of energy bands in crystals of wurtzite type: I. symmetry of bands disregarding spin-orbit interaction. *Soviet Physics, Solid State* **1**(3): 368–380.

Rashba E. 1960. Properties of semiconductors with an extremum loop. I. Cyclotron and combinational resonance in a magnetic field perpendicular to the plane of the loop. *Soviet Physics, Solid State* **2**: 1109.

Ravisankar R., Sriraman T., Salasnich L. & Muruganandam P. 2020. Quenching dynamics of the bright solitons and other localized states in spin–orbit coupled Bose–Einstein condensates. *Journal of Physics B: Atomic, Molecular and Optical Physics* **53**(19): 195301.

Rosenau P. 1994. Nonlinear dispersion and compact structures. *Physical Review Letters* **73**(13): 1737.

Rosenau P. & Hyman J.M. 1993. Compactons: solitons with finite wavelength. *Physical Review Letters* **70**(5): 564.

Rosenau P. & Schochet S. 2005. Almost compact breathers in anharmonic lattices near the continuum limit. *Physical Review Letters* **94**(4): 045503.

Sakaguchi H. & Malomed B. 2019. Nonlinear management of topological solitons in a spin-orbit-coupled system. *Symmetry* **11**(3): 388.

Salerno M. & Abdullaev F.K. 2015. Symmetry breaking of localized discrete matter waves induced by spin–orbit coupling. *Physics Letters A* **379**(37): 2252–2256.

Salerno M., Abdullaev F.K., Gammal A. & Tomio L. 2016. Tunable spin-orbit-coupled Bose-Einstein condensates in deep optical lattices. *Physical Review A* **94**(4): 043602.

Sanders J.A., Verhulst V. & Murdock J. 2007. *Averaging Methods in Nonlinear Dynamical Systems*. 2nd edn. New York: Springer Science+Business Media, LLC.

Stefanov A. & Kevrekidis P. 2012. On the existence of solitary traveling waves for generalized Hertzian chains. *Journal of Nonlinear Science* **22**: 327–349.

Struck J., Ölschläger C., Le Targat R., Soltan-Panahi P., Eckardt A., Lewenstein M., Windpassinger P. & Sengstock K. 2011. Quantum simulation of frustrated classical magnetism in triangular optical lattices. *Science* **333**(6045): 996–999.

Struck J., Ölschläger C., Weinberg M., Hauke P., Simonet J., Eckardt A., Lewenstein M., Sengstock K. & Windpassinger P. 2012. Tunable gauge potential for neutral and spinless particles in driven optical lattices. *Physical Review Letters* **108**(22): 225304.

Su J., Lyu H., Chen Y. & Zhang Y. 2021. Creating moving gap solitons in spin-orbit-coupled Bose-Einstein condensates. *Physical Review A* **104**(4): 043315.

Tononi A., Wang Y. & Salasnich L. 2019. Quantum solitons in spin-orbit-coupled Bose-Bose mixtures. *Physical Review A* **99**(6): 063618.

Vicencio R.A., Cantillano C., Morales-Inostroza L., Real B., Mejía-Cortés C., Weimann S., Szameit A. & Molina M.I. 2015. Observation of localized states in Lieb photonic lattices. *Physical review letters* **114**(24): 245503.

Wang Y.J., Wen L., Chen G.P., Zhang S.G. & Zhang X.F. 2020. Formation, stability, dynamics of vector bright solitons in Bose-Einstein condensates spin-orbit coupling. *New Journal of Physics* **22**: 033006.

Wang Y.J., Zhao X.J., Wang L.X. & Yang X.Y. 2023. Dynamics of vector bright solitons in one-dimensional Bose-Einstein condensates with time-dependent Raman coupling. *Optik - International Journal for Light and Electron Optics* **287**: 171073.

Wen L., Liang Y., Zhou J., Yu P., Xia L., Niu L.B. & Zhang X.F. 2019. Effects of linear Zeeman splitting on the dynamics of bright solitons in spin-orbit coupled Bose-Einstein condensates. *Acta Physica Sinica* **68**(8): 080301.

Yu Z.F., Chai X.D. & Xue J.K. 2018. Energetic and dynamical instability of spin–orbit coupled Bose–Einstein condensate in a deep optical lattice. *Physics Letters A* **382**(18): 1231–1237.

Zenesini A., Lignier H., Ciampini D., Morsch O. & Arimondo E. 2009. Coherent control of dressed matter waves. *Physical Review Letters* **102**(10): 100403.

Zhang A.X., Hu X.W., Jiang Y.F., Zhang Y., Zhang W. & Xue J.K. 2021. Localization and spin dynamics of spin-orbit-coupled Bose-Einstein condensates in deep optical lattices. *Physical Review E* **104**(6): 064215.

Zhang A.X., Hu X.W., Zhang W., Liang J.C. & Xue J.K. 2022. Nonlinear dynamics of tunable spin-orbit coupled Bose-Einstein condensates in deep optical lattices. *Physics Letters A* **456**: 128529.

Zhang Y., Hang C. & Huang G. 2023. Matter-wave solitons in an array of spin-orbit-coupled Bose-Einstein condensates. *Physical Review E* **108**(1): 014208.

Zhu X., Xiang D. & Zeng L. 2023. Fundamental and multipole gap solitons in spin-orbit-coupled bose-einstein condensates with parity-time-symmetric zeeman lattices. *Chaos, Solitons & Fractals* **169**: 113317.

Department of Computational and Theoretical Sciences
Kulliyyah of Science
International Islamic University Malaysia 25200 Kuantan
Pahang DM, Malaysia
E-mail: lukhman.taib@gmail.com[*]*, salihi@iium.edu.my*

Phsyical-Technical Institute
Uzbekistan Academy of Sciences
Taskhent, Bodomzor yuli, 2-b
Uzbekistan
Email: bakhram25@gmail.com

Received: 15 September 2023
Accepted: 7 Mac 2024

[*]Corresponding author